PHYSICAL REVIEW B **96**, 195121 (2017)

Correlation-driven metal-insulator transition in proximity to an iron-based superconductor

A. Charnukha,[1,*] Z. P. Yin,[2,†] Y. Song,[3] C. D. Cao,[4,3] Pengcheng Dai,[3,2] K. Haule,[5] G. Kotliar,[5] and D. N. Basov[1,6]

[1]*Physics Department, University of California-San Diego, La Jolla, California 92093, USA*
[2]*Center for Advanced Quantum Studies and Department of Physics, Beijing Normal University, Beijing 100875, China*
[3]*Department of Physics and Astronomy, Rice University, Houston, Texas 77005, USA*
[4]*Department of Applied Physics, Northwestern Polytechnical University, Xian 710072, China*
[5]*Department of Physics and Astronomy, Rutgers University, Piscataway, New Jersey 08854, USA*
[6]*Department of Physics, Columbia University, New York, New York 10027, USA*

(Received 24 April 2017; revised manuscript received 26 September 2017; published 9 November 2017)

We report the direct spectroscopic observation of a metal to correlated-insulator transition in the family of iron-based superconducting materials. By means of optical spectroscopy we demonstrate that the excitation spectrum of $NaFe_{1-x}Cu_xAs$ develops a large gap with increasing copper substitution. Dynamical mean-field theory calculations show a good agreement with the experimental data and suggest that the formation of the charge gap requires an intimate interplay of strong on-site electronic correlations and spin-exchange coupling, revealing the correlated Slater-insulator nature of the antiferromagnetic ground state. Our calculations further predict the high-temperature paramagnetic state of the same compound to be a highly incoherent correlated metal. We verify this prediction experimentally by showing that the doping-induced weakening of antiferromagnetic correlations enables a thermal crossover from an insulating to an incoherent metallic state. Redistribution of the optical spectral weight in this crossover uncovers the characteristic energy of Hund's-coupling and Mott-Hubbard electronic correlations essential for the electronic localization. Our results demonstrate that $NaFe_{1-x}Cu_xAs$ continuously transitions from the typical itinerant phases of iron pnictides to a highly incoherent metal and ultimately a correlated insulator. Such an electronic state is expected to favor high-temperature superconductivity.

DOI: 10.1103/PhysRevB.96.195121

I. INTRODUCTION

The effect of strong electronic correlations on transport properties, including superconductivity, has been one of the major research topics in condensed-matter physics for many decades [1,2]. It has been established that electronic correlations lead to increased dissipation in the electronic transport and drive itinerant electrons towards localization. These phenomena are now recognized as common attributes of high-temperature superconductivity [3–5]. While increased electronic interactions tend to stabilize a host of competing phases [6–12], they typically culminate in a completely localized correlated-insulator state.

Quite remarkably, all of the electronic phases found in the family of high-temperature iron-based superconductors are itinerant in nature [13,14], despite the presence of sizable electronic correlations [3,15–17]. Such behavior results from the multiorbital character of their electronic structure, which provides additional pathways for electrons to escape the localizing trends and effectively reduces the on-site repulsion. As a consequence, no correlated insulator has been identified in any family of Fe-based materials despite significant research efforts. This absence casts doubt onto the generality of a pervasive motif in the field of unconventional superconductivity: the proximity of the latter to a correlated insulating phase [18–20].

Here, we identify this missing link: We show that the introduction of copper at the iron sites in NaFeAs results in a fully insulating ground state with a well-defined correlation gap on the order of 0.8 eV in the antiferromagnetic state near 50% copper substitution. This observation is in stark contrast with the partially filled electronic 3*d* conduction band expected from simple electron count and unambiguously demonstrates that compounds within the family of iron-based superconductors are proximal not only to a partially localized orbitally selective Mott state [23–25] but, in fact, to a completely localized correlated-insulator phase. Based on a detailed comparison of optical spectroscopy and density-functional plus dynamical mean-field theory calculations (DFT+DMFT), we further establish that this novel electronic ground state can be described as a *correlated Slater insulator* and has no analog in condensed-matter physics. Our calculations demonstrate that the hallmark of such an electronic state is the crossover from a correlated-insulator to a paramagnetic-metal phase with highly incoherent charge transport due to large fluctuating magnetic moments, enhanced by the Hubbard (U) and Hund (J) on-site interactions. We verify this prediction and directly determine the corresponding correlation energy scales experimentally by observing such a thermal crossover in $NaFe_{1-x}Cu_xAs$ at $x = 0.3$, in which antiferromagnetic correlations have been weakened by doping.

II. EXPERIMENTAL AND THEORETICAL METHODS

A. Sample growth

High-quality single crystals of $NaFe_{1-x}Cu_xAs$ were synthesized by the self-flux method. The Cu doping levels reported in this paper were determined by inductively coupled plasma (ICP) atomic-emission spectroscopy. Samples were characterized by neutron diffraction and transport measurements [22].

*acharnukha@ucsd.edu
†yinzhiping@bnu.edu.cn

B. Optical spectroscopy measurements and data analysis

Optical-spectroscopy measurements were carried out in the range from 3 to 900 meV by means of the reflectance technique and from 0.5 to 6.5 eV using spectroscopic ellipsometry. The air-sensitive samples of $NaFe_{1-x}Cu_xAs$ were cleaved before every measurement and loaded into the measurement chamber in the neutral atmosphere of argon gas, without exposing the sample to air at any time. High-accuracy absolute measurements of the sample's reflectance were carried out using the gold-overfilling technique.

The photon-energy dependence of the optical conductivity was analyzed in the entire investigated spectral range using the following standard Drude-Lorentz model for the dielectric function [related to the optical conductivity via $\sigma(\omega) = \omega(\varepsilon(\omega) - 1)/4\pi i$]:

$$\varepsilon(\omega) = 1 - \left[\frac{4\pi\sigma_{\rm dc}\gamma}{\omega^2 + i\gamma\omega}\right]_{\rm Drude} + \left[\sum_j \frac{\Delta\varepsilon_j\omega_{0,j}^2}{\omega_{0,j}^2 - \omega^2 - i\Gamma_j\omega}\right]_{\rm interband} + \sum_{\rm k,rest}\Delta\varepsilon_k, \quad (1)$$

where the first term in the square brackets denotes the (Drude) contribution of the itinerant charge carriers, the second—the classical Lorentzian oscillators used to model the infrared-active phonons and interband transitions. The last sum accounts for the contribution of all higher-energy interband transitions (outside of the measured spectral range) to the low-energy permittivity and is usually combined with unity to give $\varepsilon_\infty = 1 + \sum_{\rm k,rest}\Delta\varepsilon_k$. The quantities in the above equation are: $\sigma_{\rm dc}$ and γ are the dc conductivity and the quasiparticle scattering rate; $\Delta\varepsilon_j\omega_{0,j}^2$ is the oscillator strength f_j of the jth term in units of $4\pi e^2/m_e$ (e and m_e are the electron charge and mass, respectively); $\omega_{0,j}$ is the center frequency and Γ is the linewidth of the jth Lorentzian term. The itinerant spectral weight plotted in Fig. 1 is defined as the total area under the itinerant conductivity curve $\int_0^\infty \Re\sigma^{\rm Drude}(\Omega)d\Omega = \int_0^\infty (4\pi)^{-1}\Im\varepsilon^{\rm Drude}(\Omega)\Omega d\Omega = (\pi/2)\sigma_{\rm dc}\gamma$, where $\Re,\Im$ denote the real and imaginary part of a complex-valued function.

C. DFT+DMFT calculations

Density functional theory (DFT) calculations were done using the full-potential linear augmented plane wave method implemented in WIEN2K (Ref. [26]) in conjunction with a generalized gradient approximation [27] of the exchange correlation functional. To take into account strong correlation effects, we further carried out first-principles calculations using a combination of density functional theory and dynamical mean field theory (DFT+DMFT) (Ref. [28]) which was implemented on top of WIEN2K as documented in Ref. [29]. In the DFT+DMFT calculations, the electronic charge was computed self-consistently on DFT+DMFT density matrix. The quantum impurity problem was solved by the continuous time quantum Monte Carlo (CTQMC) method [30,31], using the Slater form of the Coulomb repulsion in its fully rotational invariant form. Double counting of the electronic interactions was treated exactly [32].

We used a Hubbard $U = 8.0$ eV and Hund's rule coupling $J = 0.9$ eV in both paramagnetic and antiferromagnetic states

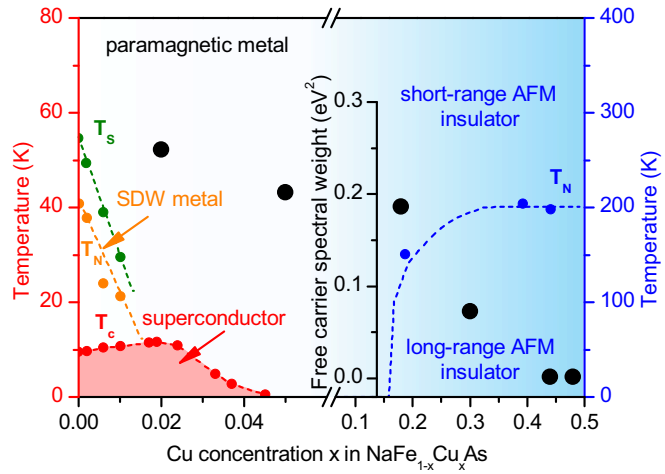

FIG. 1. Phase diagram of $NaFe_{1-x}Cu_xAs$. Below $x = 0.05$ $NaFe_{1-x}Cu_xAs$ shows the ubiquitous phases of iron-based compounds (left axis): superconductivity (red symbols, line, and shaded area), SDW order (orange symbols and line), and a tetragonal-to-orthorhombic structural transition ~10 K above $T_{\rm SDW}$ (green symbols and line). Data after Ref. [21]. At high doping levels, $NaFe_{1-x}Cu_xAs$ exhibits real-space ordering of copper and iron ions [see Fig. 4(b)] and an antiferromagnetic phase transition (blue symbols and line, right axis). Data after Ref. [22]. In this paper we find that upon increasing copper concentration, a metal-insulator transition (MIT) occurs, gapping the Fe-3d states and eliminating itinerant SW (black symbols, middle axis).

since the iron atom is close to a 3+ state (i.e., with five Fe 3d electrons), consistent with our previous treatment of the isostructural and isovalent compound LaMnPO (Ref. [33]), and experimentally determined crystal structure, including the internal positions of the atoms [22]. We further took into account the real-space ordering of Fe and Cu ions identified in $NaFe_{1-x}Cu_xAs$ near the $x = 0.5$ substitution level [22] by implementing a corresponding supercell. As will be shown in the next section, the difference in the optical properties between the $x = 0.44$ and $x = 0.48$ compounds is negligible, implying that disorder does not have a strong effect on the ground state properties of $NaFe_{1-x}Cu_xAs$ in this regime and our $x = 0.5$ fully ordered supercell calculation is justified. Our DFT+DMFT method improves the DFT description of the electronic structure of iron-based superconductors, predicts the correct magnitude of the ordered magnetic moments [16], and improves the description of electronic spectral functions, Fermi surfaces [34], charge response functions such as the optical conductivity [35], and magnetic response functions such as the dynamical spin susceptibility [36].

III. RESULTS AND DISCUSSION

A. Doping-induced metal-insulator crossover

Figure 1 shows the insulating and metallic phases and the magnitude of itinerant spectral weight (SW) at room temperature determined in the present work superimposed onto the phase diagram of $NaFe_{1-x}Cu_xAs$. At low doping levels superconductivity emerges from a high-temperature metallic phase and reaches optimum once the SDW order of

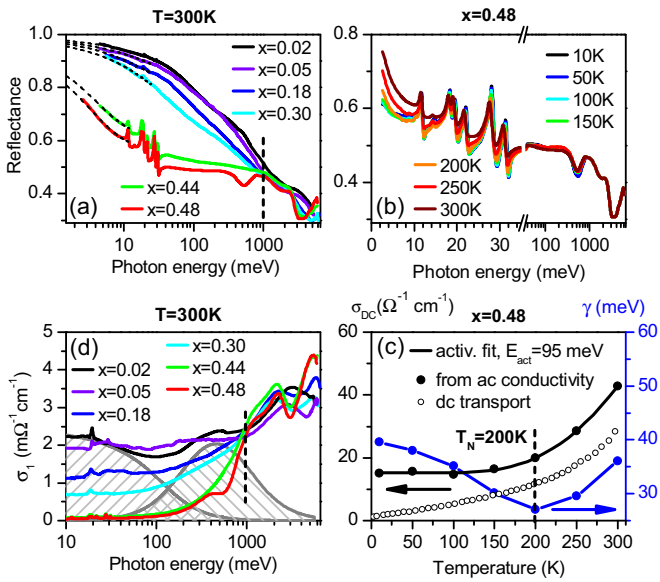

FIG. 2. (a) Energy dependence of $NaFe_{1-x}Cu_xAs$ reflectance for $x = 0.02$ (black), 0.05 (purple), $x = 0.18$ (blue), 0.30 (cyan), 0.44 (green), and 0.48 (red solid line) at $T = 300$ K. Dashed lines indicate the low-energy single-band Drude fit. (b) Temperature dependence of $NaFe_{1-x}Cu_xAs$ reflectance for $x = 0.48$. Gradual suppression of the reflectance at lowest energies with decreasing temperature indicates the thermally activated character of the low-energy response. (c) Temperature dependence of the directly measured dc conductivity (open symbols, from Ref. [22]) and the corresponding quantity (black filled symbols) extracted from a Drude-Lorentz analysis of the infrared reflectance in panel (b) (for details see Ref. [38]). The quasiparticle scattering rate obtained in the same analysis (blue filled symbols). Dashed vertical line indicates the Néel transition temperature determined by means of neutron diffraction on the same compound in Ref. [22]. (d) Real part of the optical conductivity at $T = 300$ K as a function of photon energy for the same doping levels as in panel (a). Vertical dashed line shows the characteristic energy scale of the SW transfer from low to high energies with increasing copper substitution. This SW is composed of two main contributions: itinerant intraband (Drude term, left hatched area) and Fe-d–Fe-d interband (Lorentz oscillator, right hatched area) optical transitions.

the parent compound has been sufficiently suppressed [21]. At doping levels near $x = 0.5$ $NaFe_{1-x}Cu_xAs$ exhibits insulating behavior in the dc resistivity up to room temperature [21,22,37] with an activation energy on the order of 10 meV. In the same region of the phase diagram neutron diffraction investigations have revealed the presence of real-space ordering of nonmagnetic copper and magnetic iron ions into alternating stripes [22] [see Fig. 4(b)] and the development of long-range antiferromagnetic order on iron sites below 200 K.

In order to elucidate the nature of the MIT in $NaFe_{1-x}Cu_xAs$ with doping, we investigate multiple compositions spanning the entire phase diagram by means of optical spectroscopy. This technique allows one to probe directly the most conspicuous signatures of the metallic and insulating state of matter—the itinerant SW and the energy gap, respectively. Figure 2(a) shows that upon the transition from the low-doping metallic to the high-doping insulating regime, the far-infrared reflectance of $NaFe_{1-x}Cu_xAs$ experiences a dramatic suppression up to ≈1 eV evidencing the appearance of an energy gap and occurrence of high-energy SW transfer. In the $x = 0.48$ compound this suppression is fully preserved up to room temperature, as shown in Fig. 2(b). The small changes in the reflectance below 100 meV are entirely due to the thermal excitation of charge carriers. The activated character of the low-energy response is evident in the temperature dependence of $\sigma_1(\omega \to 0)$ plotted in Fig. 2(c). This quantity corresponds to the dc limit of the optical conductivity and has been extracted from a Drude-Lorentz fit of the reflectance data in Fig. 2(b). Using the Arrhenius fit we obtain an activation energy of ≈100 meV. The temperature dependence of $\sigma_1(\omega \to 0)$ displays no anomalies around the Néel transition temperature, indicating that the electronic band structure is unchanged across T_N. This observation is consistent with the recent results of angle-resolved photoemission spectroscopy (ARPES) on the same compound [37]. The high-temperature behavior of σ_{dc}, determined in the transport measurements in Ref. [22], follows that of $\sigma_1(\omega \to 0)$ very closely and starts to deviate around 100 K ≈ 8 meV, indicating the presence of very shallow impurity states. Unlike the temperature dependence of $\sigma_1(\omega \to 0)$, that of the quasiparticle scattering rate γ, extracted in the same fit, exhibits a clear anomaly around T_N due to the modification of the scattering channels upon the long-range ordering of local Fe magnetic moments. The anomaly has the character of a broad crossover, suggesting that antiferromagnetism does not vanish entirely at T_N but persists on short length scales.

The redistribution of the itinerant SW from low to high energies accounts for only a part of the total redistribution between the metallic and insulating compounds. To better understand what optical transitions are affected by copper substitution in $NaFe_{1-x}Cu_xAs$, we extract the optical conductivity by means of the Kramers-Kronig transformation of the reflectance data presented in Fig. 2(a). Figure 2(d) shows that the strong itinerant response dominating the low-energy real part of the optical conductivity of the metallic $x = 0.02$ and $x = 0.05$ samples [left hatched area in Fig. 2(d)] is gradually suppressed in the $x = 0.18$ and $x = 0.30$ compounds and entirely eliminated at $x = 0.44$ and $x = 0.48$ substitution due to the opening of an excitation gap in the electronic band structure. However, it is evident that the copper substitution likewise strongly affects the ubiquitous in iron pnictides 0.5 eV absorption band [40], which stems from transitions between Fe-3d states [38]. This band shifts to higher energies and shapes an absorption edge in the insulating $NaFe_{1-x}Cu_xAs$ indicating that the DOS up to about 1 eV experiences substantial suppression. The detailed analysis of the optical conductivity is presented in the next section.

B. Analysis of the correlation energy gap

In order to determine the characteristic energy of the absorption edge, we plot the quantity $(\varepsilon_2(\omega)\omega^2)^2$ (ε_2 and $\hbar\omega$ are the imaginary part of the dielectric function and photon energy, respectively). Figure 3(a) shows that this quantity exhibits linear behavior with an intercept with the horizontal axis at about $E_{dir,1} \approx 0.8$ eV in both the $x = 0.44$ and $x = 0.48$ compound, indicative of the direct character of the band gap [39]. Another direct band gap edge is evident at higher energies,

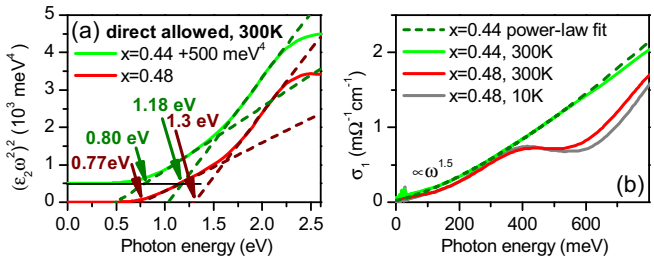

FIG. 3. (a) Energy dependence of $(\varepsilon_2\omega^2)^2$ in $NaFe_{1-x}Cu_xAs$ for $x = 0.48$ and $x = 0.44$ (offset vertically by 500 meV^4 for clarity) at $T = 300$ K. Linear segments (dashed lines) in this quantity are characteristic of direct allowed interband transitions [39]. The corresponding absorption edges are given by the intercepts of the linear dependence with the horizontal axis and are indicated by arrows. (b) Low-energy part of the optical conductivity shown in Fig. 2(d) below the lowest direct absorption edge identified in panel (a) for $x = 0.44$ at $T = 300$ K (green line) and $x = 0.48$ at $T = 300$ K (red line) and, additionally, at $T = 10$ K (gray line). The energy dependence at $x = 0.44$ can be approximated by a power law with an exponent of 1.5 over an extended spectral range (dashed line) and at $x = 0.48$ over a somewhat narrower range.

with $E_{\mathrm{dir},2} \approx 1.2$ eV. Figure 2(d) shows that the energy $E_{\mathrm{dir},1}$ only defines a soft absorption edge due to the presence of substantial absorption tail below this energy. The frequency dependence of the optical conductivity in this tail is shown in detail in Fig. 3(b) and follows a power-law behavior with an exponent of about 1.5. The corresponding optical transitions likely involve bands with a low density of states as well as localized electronic states. The true hard band edge is characterized by the activation energy of 100 meV determined above.

C. Theoretical analysis of the insulating state

In order to shed light onto the microscopic origin of the charge localization, we have carried out DFT+DMFT calculations of three main electronic states relevant to the present discussion: paramagnetic NaFeAs ($x = 0$) and $NaFe_{0.5}Cu_{0.5}As$, as well as antiferromagnetically ordered $NaFe_{0.5}Cu_{0.5}As$ with a real-space Cu-Fe stripe superstructure [see Fig. 4(b)] observed experimentally by neutron diffraction [22]. This superstructure and magnetic order are to be compared with the low-temperature spin-density-wave (SDW) stripe antiferromagnetic order of the parent compound NaFeAs (Ref. [41]) shown in Fig. 4(a). The ordered magnetic moment of Fe ions in the SDW phase of NaFeAs has been found to lie between 0.09 and 0.32 μ_B (Refs. [41–43]), much smaller than a fully localized moment 4 μ_B in the Fe-3d^6 electronic configuration. This discrepancy is the direct consequence of the partially itinerant nature of the magnetic state [16]. The ordered magnetic moment on the Fe ions in the antiferromagnetic state of $NaFe_{0.5}Cu_{0.5}As$ reaches 1.1 μ_B (Ref. [22])—substantially higher than in the parent compound, consistent with a more local origin of the magnetism. It remains well below the fully localized moment of 5 μ_B expected in the Fe-3d^5 electronic configuration, implying that charge fluctuations remain important even in the fully localized ground state of $NaFe_{0.5}Cu_{0.5}As$.

Figures 4(c)–4(e) illustrate the evolution of the partial density of states (pDOS) of $NaFe_{1-x}Cu_xAs$ upon increasing copper substitution from $x = 0$ to $x = 0.5$ and the effect of antiferromagnetic ordering on the states near the Fermi level (E_F). Most of the Cu-3d states appear at high binding energies below E_F and contribute little to the conduction band. This observation is consistent with the fully occupied Cu-3d^{10} electronic configuration reported earlier [22,44]. The pDOS of Fe-3d orbitals is high near E_F, implying that the $x = 0.5$ compound in our calculations [Fig. 4(d)] is almost purely an Fe-3d metal in the paramagnetic state with a large itinerant SW, similarly to the parent NaFeAs [Fig. 4(c)]. The introduction of antiferromagnetic order changes the situation dramatically: A large soft gap on the order of 0.8 eV opens around E_F, in excellent agreement with the experimentally obtained value.

A more detailed insight into the effect of magnetic ordering on the electronic state can be obtained by examining the band dispersions in the paramagnetic and antiferromagnetic state presented in Figs. 4(f) and 4(g) in the form of the ARPES spectral function. Such a representation reveals not only band renormalization induced by electronic interactions (real part of the quasiparticle self-energy) but also the interaction-induced broadening of the quasiparticle peak (imaginary part of the quasiparticle self-energy). Figure 4(f) shows that quasiparticles in the paramagnetic state of the $x = 0.5$ compound are extremely incoherent: There are no sharp quasiparticle peaks in the vicinity of E_F. This incoherence results from the scattering of electrons by strong antiferromagnetic fluctuations. We would like to emphasize that despite this dramatic broadening, the itinerant SW remains substantial, resulting in a pronounced bad metal behavior.

In the antiferromagnetically ordered state [Fig. 4(g)], on the other hand, the aforementioned fluctuations become quenched and the electronic bands experience exchange splitting. The occupied states of this electronic band structure are in good agreement with the results of ARPES measurements on the same compound [37]. This band structure further reveals that the soft absorption edge identified earlier is formed by flat valence and conduction bands separated by 0.8 eV. The corresponding magnified pDOS is shown in Fig. 4(h). The states below this edge are contributed by a single hole valence band with a very small DOS, consistent with the experimental optical conductivity spectrum in Fig. 2(d). Figures 4(g) and 4(h) further show a clear hard direct band gap of about 100 meV at the M point of the Brillouin zone, in excellent agreement with the same value of the activation energy extracted from the temperature dependence of $\sigma_1(\omega \to 0)$ in Fig. 2(c). A slightly smaller indirect band gap is present in the band structure but was not detected in our measurements, possibly due to the very low DOS of the forming bands.

We find other possible sources of the charge gap, such as charge disproportionation and Anderson-Hubbard localization [45–47] of correlated electrons due to lattice defects rather unlikely. The former is hard to reconcile with the nearly Fe-3d^5 and Cu-3d^{10} electronic configuration established in $NaFe_{0.5}Cu_{0.5}As$ (Ref. [22]), which implies that all Fe ions exhibit the same 3+ valency. Anderson localization in a strongly correlated electron system is incompatible with the nearly complete suppression of the itinerant SW on the energy scale of 0.8 eV. Furthermore, we note that the amount of

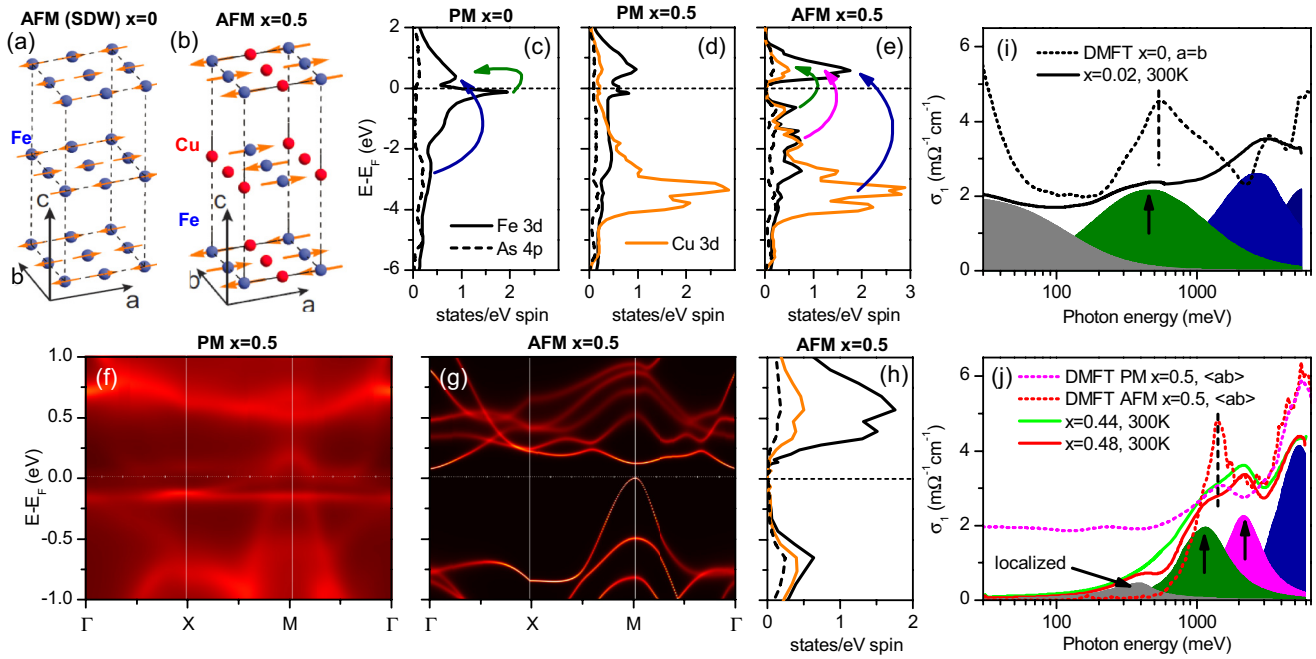

FIG. 4. (a),(b) The arrangement of the magnetic moments in the antiferromagnetic ground state of $NaFe_{1-x}Cu_xAs$ in the itinerant parent $x = 0$ (a) and localized $x = 0.5$ (b) compound (after Refs. [22,41]). Nonmagnetic arsenic ions are excluded for clarity. (c),(d) Evolution of the pDOS near E_F in the band structure of $NaFe_{1-x}Cu_xAs$ calculated using DFT+DMFT in the paramagnetic state upon increasing copper substitution from $x = 0$ (c) to $x = 0.5$ (d). (e) Same for the antiferromagnetic ground state at $x = 0.5$. Arrows in (c) and (e) indicate dominant interband optical transitions. (f),(g) Simulated distribution of ARPES intensity in an energy-momentum cut along several high-symmetry directions in the Brillouin zone for the paramagnetic (f) and antiferromagnetic (g) state at $x = 0.5$. (h) The corresponding enlarged pDOS from panel (e) obtained in the same calculation (h). The presence of a soft gap of order 0.8 eV is evident in the pDOS (h). (i),(j) Comparison of the experimental (solid lines) and theoretical (dashed lines) optical conductivity spectra of $NaFe_{1-x}Cu_xAs$ at $x = 0$ (i) and $x = 0.5$ (j). Shaded areas indicate the itinerant (intraband) and localized (interband) contributions to the optical conductivity extracted by means of a Drude-Lorentz analysis (see Ref. [38]). Vertical arrows and dashed lines show the center location of the lowest-lying clearly identifiable interband optical transition in both experimental and theoretical optical conductivity. Theoretical in-plane optical conductivity spectra for the $x = 0.5$ compound in the direction of the a and b crystal axis were averaged to take into account domain twinning [22].

disorder in $NaFe_{0.5}Cu_{0.5}As$ is very small due to the real-space ordering of Fe and Cu ions (see Fig. 4(b) and Ref. [22]). The high degree of crystalline order is further confirmed by the relatively sharp quasiparticle peaks observed in the ARPES measurements on the same compound in the antiferromagnetic state [37].

It is important to note that antiferromagnetic order alone in the absence of strong electronic correlations is insufficient to open a full gap in the electronic structure of $NaFe_{0.5}Cu_{0.5}As$ (see Fig.S2 in Ref. [37]). Similarly, in the absence of antiferromagnetism, this material remains (at least partially) conductive for all physically reasonable magnitudes of electronic interaction strength (We would like to note that a previous calculation using an entirely different, slave-spin, approach [22] did achieve insulating behavior also in the absence of antiferromagnetism.). The assumed periodic arrangement of the Cu ions and the resulting superlattice could, in principle, produce a (pseudo)gap in the electronic structure. This is indeed the case in some parameter range of our calculations. However, such a (pseudo)gap only opens in the direction perpendicular to the iron and copper chains, where hopping is modified. Experimentally, given the presence of twin domains with the mutually orthogonal direction of the Fe and Cu chains [22], the existence of an insulating and metallic direction would necessarily be evident in finite effective optical conductivity below the gap. Our experimental results explicitly exclude such a scenario as no substantial optical conductivity is present in the $x = 0.44$ and $x = 0.48$ compounds at any photon energy below the gap [see Fig. 2(d)].

In addition to the very good agreement of the general energetics of the electronic structure between experiment and theory discussed above, the predicted optical conductivity aligns reasonably well with the data in Fig. 2(d). Figure 4(i) shows the comparison of the calculated ($x = 0$) and measured ($x = 0.02$) optical conductivity in metallic $NaFe_{1-x}Cu_xAs$. Theory reproduces all of the main spectral features: the characteristic for iron pnictides strong and incoherent itinerant response [40]; absorption band centered near 0.5 eV and modified from the DFT value by a typical bandwidth renormalization factor of 2–3 (Ref. [48]); higher-energy interband transitions. The corresponding dominant optical transitions are shown in Fig. 4(c) with arrows [arrow colors match the colors of the filled areas in Fig. 4(i)]. Analogous comparison of the theoretically predicted optical conductivity of the $x = 0.5$ compound in the antiferromagnetic state and its experimental counterpart at 300 K (the temperature dependence of the optical conductivity is negligible above 100 meV) shows an even better agreement [Fig. 4(j)]. The corresponding

dominant optical transitions are shown in Fig. 4(e) with colored arrows.

Figure 4(j) further shows our calculated optical conductivity spectrum for the paramagnetic state of the $x = 0.5$ compound (magenta dashed line), corresponding to the ARPES spectral function and pDOS in Figs. 4(f) and 4(d). This electronic state is yet to be observed experimentally and requires the obliteration of short-range antiferromagnetism. The optical conductivity spectrum reveals that the itinerant response of the $x = 0.5$ compound in the metallic paramagnetic state is comparable to that of parent NaFeAs. The MIT at $x = 0.5$ would thus involve characteristic interaction energies on the order of 1 eV, in an excellent agreement with the same characteristic energy of the doping-induced MIT directly identified in our experiment as shown in Figs. 2(a) and 2(d).

D. Thermal crossover from a metal to a correlated insulator

While the complete suppression of short-range antiferromagnetism and recovery of the predicted highly incoherent metallic state in the $x \approx 0.5$ compound will require temperatures well in excess of ambient, one may expect such a thermal metal to correlated-insulator crossover to occur in the vicinity of room temperature once the antiferromagnetism has been sufficiently weakened by doping. Indeed, the phase diagram in Fig. 1 reveals that the antiferromagnetic long-range ordering temperature is gradually suppressed below the $x = 0.44$ substitution level. We have investigated the temperature dependence of the optical properties of the $x = 0.3$ compound down to 10 K and have found clear evidence for a thermal metal-insulator crossover. The reflectance of this material, displayed in Fig. 5(a), shows a pronounced suppression upon decreasing temperature of the same order of magnitude as that due to the doping-induced metal-insulator transition in Fig. 2(a). Furthermore, these changes have a characteristic energy scale of about 0.6 eV (dashed vertical line in Fig. 5), likewise comparable to the doping-induced case. The temperature dependence of the material's reflectance at a photon energy of 10 meV in Fig. 5(b) shows an almost linear behavior without signs of saturation near room temperature. Such a behavior is in stark contrast to the simple thermal activation of charge carriers observed in the $x = 0.48$ compound [Figs. 2(b) and 2(c)] and implies a correlation-driven depletion of itinerant charge carriers. The absence of any discernible anomalies around the Néel transition temperature [gray shaded area in Fig. 5(b)] further confirms the persistence of short-range antiferromagnetic order well above the long-range ordering temperature T_N and its gradual suppression in a thermal crossover.

The temperature dependence of the optical conductivity of the $x = 0.3$ compound shown in Fig. 5(c) makes the dramatic suppression of the itinerant charge-carrier response in this thermal crossover even more explicit. The spectral shape of the optical conductivity at 300 K is flat up to the onset of interband absorption, consistent with a highly incoherent, bad-metal, behavior predicted in our DFT+DMFT calculations for the paramagnetic state of the $x = 0.5$ compound. It further reveals the vanishing of a large amount of itinerant spectral weight in the infrared spectral range upon cooling (hatched area). Due to the conservation of the total optical spectral weight imposed by the optical sum rule, this missing area

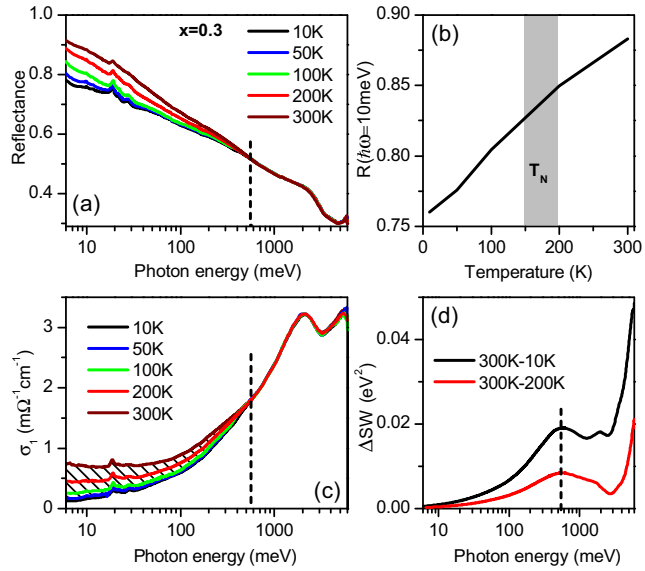

FIG. 5. (a) Energy dependence of $NaFe_{1-x}Cu_xAs$ reflectance for $x = 0.3$ at various temperatures. Vertical dashed line indicates the energy scale beyond which the temperature-induced changes in infrared reflectance largely vanish. (b) Temperature dependence of reflectance at 10 meV photon energy. Gray shaded area indicates the temperature window for the Néel transition temperature in this compound (according to the phase diagram in Fig. 1). (c) Energy dependence of the real part of the optical conductivity at various temperatures. Dashed vertical line as in panel (a). Hatched area indicates the missing infrared spectral weight between 300 K and 10 K. (d) Energy dependence of the difference partial spectral weight between room temperature and 200 K (red line) as well as 10 K (black line).

must be regained at higher energies. The energy at which compensation occurs corresponds to a characteristic energy of the interaction responsible for the observed spectral-weight redistribution. We plot in Fig. 5(d) the difference partial spectral weight defined as $\Delta SW(\omega,T) = SW(\omega,300\text{ K}) - SW(\omega,T) = \int_0^{\omega} [\sigma_1(\Omega,300\text{ K}) - \sigma_1(\Omega,T)]d\Omega$ for two temperatures: 200 and 10 K. One can see that the characteristic energy scale indicated with vertical dashed lines in Figs. 5(a) and 5(c) corresponds to the saturation in the accumulation of the lost spectral weight. While a portion of the missing spectral weight is recovered by 3 eV, no full compensation occurs within our measurement's spectral range, up to 6.5 eV. High-energy local interactions must, therefore, participate in the metal to correlated-insulator thermal crossover observed in this compound.

Our experimental findings and DFT+DMFT calculations suggest that the insulating ground state in $NaFe_{1-x}Cu_xAs$ results from the exchange splitting of the low-energy band structure in the antiferromagnetic state, which persists on short length scales and vanishes in a crossover above T_N. The magnitude of the exchange splitting as well as the energy gap in the optical excitation spectrum is determined by strong on-site electronic correlations of the Hund ($J = 0.9$ eV) and Hubbard ($U = 8.0$ eV) type in the nearly half-filled Fe-$3d^5$ configuration. We have experimentally observed these characteristic energy scales directly in the optical conductivity across

the doping-induced and thermal metal-insulator crossover. Our findings demonstrate that $NaFe_{1-x}Cu_xAs$ at $x \approx 0.5$ may be considered proximal to a maximally correlated iron pnictide in the sense that the Hund's-rule and Hubbard electronic correlations are sufficiently strong to fully localize itinerant charge carriers in the antiferromagnetic state and make charge transport extremely incoherent in the paramagnetic state. These aspects imply the existence of intense antiferromagnetic spin fluctuations strongly coupled to itinerant charge carriers—a situation well known to promote high-temperature superconductivity.

ACKNOWLEDGMENTS

We would like to thank K. W. Post, M. D. Goldflam, and J. P. Hinton for their assistance in sample handling. A.C. acknowledges financial support by the Alexander von Humboldt foundation. Work at the University of California, San Diego and Columbia University is supported by NSF Grant No. DMR1609096. D.N.B. is the Gordon and Betty Moore Foundation investigator in Quantum Materials, EPIQS Initiative Grant GBMF4533. Z.P.Y. acknowledges financial support by the National Natural Science Foundation of China, Grant No. 11674030, National Key Research and Development Program of China under Contract No. 2016YFA0302300, and National Youth Thousand Talent Program of China. Single-crystal synthesis efforts at Rice University are supported by the US DOE, Office of Basic Energy Sciences, under Contract No. DE-SC0012311 (P.D.). Part of the materials work at Rice University is supported by the Robert A. Welch Foundation Grant No. C-1839 (P.D.). C.D.C. acknowledges financial support by the National Natural Science Foundation of China Grant No. 51471135, the National Key Research and Development Program of China under Contract No. 2016YFB1100101, and Key Research and Development Program of Shaanxi under Contract No. 2017KW-ZD-07.

[1] N. F. Mott, Rev. Mod. Phys. **40**, 677 (1968).
[2] E. Dagotto, Rev. Mod. Phys. **66**, 763 (1994).
[3] M. M. Qazilbash, J. J. Hamlin, R. E. Baumbach, L. Zhang, D. J. Singh, M. B. Maple, and D. N. Basov, Nat. Phys. **5**, 647 (2009).
[4] D. N. Basov and A. V. Chubukov, Nat. Phys. **7**, 272 (2011).
[5] S. A. Hartnoll, Nat. Phys. **11**, 54 (2015).
[6] D. Vaknin, S. K. Sinha, D. E. Moncton, D. C. Johnston, J. M. Newsam, C. R. Safinya, and H. E. King, Phys. Rev. Lett. **58**, 2802 (1987).
[7] Y. Kohsaka, T. Hanaguri, M. Azuma, M. Takano, J. C. Davis, and H. Takagi, Nat. Phys. **8**, 534 (2012).
[8] G. Ghiringhelli, M. Le Tacon, M. Minola, S. Blanco-Canosa, C. Mazzoli, N. B. Brookes, G. M. De Luca, A. Frano, D. G. Hawthorn, F. He, T. Loew, M. Moretti Sala, D. C. Peets, M. Salluzzo, E. Schierle, R. Sutarto, G. A. Sawatzky, E. Weschke, B. Keimer, and L. Braicovich, Science **337**, 821 (2012).
[9] S. Blanco-Canosa, A. Frano, T. Loew, Y. Lu, J. Porras, G. Ghiringhelli, M. Minola, C. Mazzoli, L. Braicovich, E. Schierle, E. Weschke, M. Le Tacon, and B. Keimer, Phys. Rev. Lett. **110**, 187001 (2013).
[10] M. Hashimoto, I. M. Vishik, R.-H. He, T. P. Devereaux, and Z.-X. Shen, Nat. Phys. **10**, 483 (2014).
[11] M. H. Hamidian, S. D. Edkins, S. H. Joo, A. Kostin, H. Eisaki, S. Uchida, M. J. Lawler, E.-A. Kim, A. P. Mackenzie, K. Fujita, J. Lee, and J. C. S. Davis, Nature (London) **532**, 343 (2016).
[12] R. Landig, L. Hruby, N. Dogra, M. Landini, R. Mottl, T. Donner, and T. Esslinger, Nature (London) **532**, 476 (2016).
[13] P. Dai, J. Hu, and E. Dagotto, Nat. Phys. **8**, 709 (2012).
[14] P. Dai, Rev. Mod. Phys. **87**, 855 (2015).
[15] Q. Si and E. Abrahams, Phys. Rev. Lett. **101**, 076401 (2008).
[16] Z. P. Yin, K. Haule, and G. Kotliar, Nat. Mater. **10**, 932 (2011).
[17] Q. Si, R. Yu, and E. Abrahams, Nat. Rev. Mater. **1**, 16017 (2016).
[18] B. Keimer, S. A. Kivelson, M. R. Norman, S. Uchida, and J. Zaanen, Nature (London) **518**, 179 (2015).
[19] P. Gegenwart, Q. Si, and F. Steglich, Nat. Phys. **4**, 186 (2008).
[20] O. Gunnarsson, Rev. Mod. Phys. **69**, 575 (1997).
[21] A. F. Wang, J. J. Lin, P. Cheng, G. J. Ye, F. Chen, J. Q. Ma, X. F. Lu, B. Lei, X. G. Luo, and X. H. Chen, Phys. Rev. B **88**, 094516 (2013).
[22] Y. Song, Z. Yamani, C. Cao, Y. Li, C. Zhang, J. S. Chen, Q. Huang, H. Wu, J. Tao, Y. Zhu, W. Tian, S. Chi, H. Cao, Y.-B. Huang, M. Dantz, T. Schmitt, R. Yu, A. H. Nevidomskyy, E. Morosan, Q. Si, and P. Dai, Nat. Commun. **7**, 13879 (2016).
[23] R. Yu and Q. Si, Phys. Rev. Lett. **110**, 146402 (2013).
[24] M. Yi, D. H. Lu, R. Yu, S. C. Riggs, J.-H. Chu, B. Lv, Z. K. Liu, M. Lu, Y.-T. Cui, M. Hashimoto, S.-K. Mo, Z. Hussain, C. W. Chu, I. R. Fisher, Q. Si, and Z.-X. Shen, Phys. Rev. Lett. **110**, 067003 (2013).
[25] Z. Wang, M. Schmidt, J. Fischer, V. Tsurkan, M. Greger, D. Vollhardt, A. Loidl, and J. Deisenhofer, Nat. Commun. **5**, 3202 (2014).
[26] P. Blaha, K. Schwarz, G. Madsen, D. Kvasnicka, and J. Luitz, WIEN2K, *An Augmented Plane Wave+Local Orbitals Program for Calculating Crystal Properties* (Karlheinz Schwarz, Techn. Universität Wien, Austria, 2001).
[27] J. P. Perdew, K. Burke, and M. Ernzerhof, Phys. Rev. Lett. **77**, 3865 (1996).
[28] G. Kotliar, S. Y. Savrasov, K. Haule, V. S. Oudovenko, O. Parcollet, and C. A. Marianetti, Rev. Mod. Phys. **78**, 865 (2006).
[29] K. Haule, C.-H. Yee, and K. Kim, Phys. Rev. B **81**, 195107 (2010).
[30] K. Haule, Phys. Rev. B **75**, 155113 (2007).
[31] P. Werner, A. Comanac, L. de' Medici, M. Troyer, and A. J. Millis, Phys. Rev. Lett. **97**, 076405 (2006).
[32] J. Lee and K. Haule, Phys. Rev. B **91**, 155144 (2015).
[33] D. E. McNally, J. W. Simonson, K. W. Post, Z. P. Yin, M. Pezzoli, G. J. Smith, V. Leyva, C. Marques, L. DeBeer-Schmitt, A. I. Kolesnikov, Y. Zhao, J. W. Lynn, D. N. Basov, G. Kotliar, and M. C. Aronson, Phys. Rev. B **90**, 180403(R) (2014).
[34] Z. P. Yin, K. Haule, and G. Kotliar, Nat. Phys. **7**, 294 (2011).
[35] Z. P. Yin, K. Haule, and G. Kotliar, Phys. Rev. B **86**, 195141 (2012).
[36] Z. P. Yin, K. Haule, and G. Kotliar, Nat. Phys. **10**, 845 (2014).
[37] C. E. Matt, N. Xu, B. Lv, J. Ma, F. Bisti, J. Park, T. Shang, C. Cao, Y. Song, A. H. Nevidomskyy, P. Dai, L. Patthey, N. C. Plumb, M. Radovic, J. Mesot, and M. Shi, Phys. Rev. Lett. **117**, 097001 (2016).

[38] A. Charnukha, O. V. Dolgov, A. A. Golubov, Y. Matiks, D. L. Sun, C. T. Lin, B. Keimer, and A. V. Boris, Phys. Rev. B **84**, 174511 (2011).
[39] P. Y. Yu and M. Cardona, *Fundamentals of Semiconductors* (Springer, Berlin, 2005).
[40] A. Charnukha, J. Phys.: Condens. Matter **26**, 253203 (2014).
[41] S. Li, C. de la Cruz, Q. Huang, G. F. Chen, T. L. Xia, J. L. Luo, N. L. Wang, and P. Dai, Phys. Rev. B **80**, 020504(R) (2009).
[42] G. Tan, Y. Song, C. Zhang, L. Lin, Z. Xu, T. Hou, W. Tian, H. Cao, S. Li, S. Feng, and P. Dai, Phys. Rev. B **94**, 014509 (2016).
[43] L. Ma, G. F. Chen, D.-X. Yao, J. Zhang, S. Zhang, T.-L. Xia, and W. Yu, Phys. Rev. B **83**, 132501 (2011).
[44] S. T. Cui, S. Kong, S. L. Ju, P. Wu, A. F. Wang, X. G. Luo, X. H. Chen, G. B. Zhang, and Z. Sun, Phys. Rev. B **88**, 245112 (2013).
[45] R. Vlaming and D. Vollhardt, Phys. Rev. B **45**, 4637 (1992).
[46] V. Dobrosavljević and G. Kotliar, Phys. Rev. Lett. **78**, 3943 (1997).
[47] K. Byczuk, W. Hofstetter, and D. Vollhardt, Phys. Rev. Lett. **94**, 056404 (2005).
[48] A. Charnukha, P. Popovich, Y. Matiks, D. L. Sun, C. T. Lin, A. N. Yaresko, B. Keimer, and A. V. Boris, Nat. Commun. **2**, 219 (2011).